Applied Thermal Engineering 249 (2024) 123418

Contents lists available at ScienceDirect

Applied Thermal Engineering

journal homepage: www.elsevier.com/locate/apthermeng

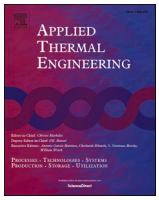

Research Paper

Enhanced monitoring and dynamic analysis of a concentrated solar thermal experimental plant for steam production

Marco A. David-Hernández [a,*], Antonio Cazorla-Marín [a], José Gonzálvez-Maciá [a], Jorge Payá-Herrero [a], Miguel Frasquet [b]

[a] Instituto Universitario de Investigación de Ingeniería Energética (IUIIE), Universitat Politècnica de València, Camino de vera sn, 46022 València, Spain
[b] SOLATOM CSP, Pedro Duque 7, 46022 València, Spain

ARTICLE INFO

Keywords:
Solar process heat
Concentrated solar thermal
Uncertainty analysis
System monitoring

ABSTRACT

Solar heat for industrial processes (SHIP) is an increasingly interest option as a key strategy to decarbonise the industrial sector. Linear Fresnel Collectors are a promising technology due to their cost-effectiveness and efficiency. As part of the SOLPINVAP project, an experimental facility was constructed to prove the use of modular Linear Fresnel collectors for steam production in industrial processes. SHIP plants commonly use standard industrial sensors, which can result in high uncertainty when measuring absorbed and produced heat. This can be problematic when selling energy to customers through an energy purchase agreement. To address this issue, an uncertainty analysis was conducted in the experimental plant, and more precise instrumentation was added to the installation. This reduced the uncertainty in the absorbed energy in the solar field from 12 % to 3 % and obtaining an uncertainty of 3 % in the generated energy. Additionally, the operation of the plant was studied through experimental tests conducted during the summer of 2022, and the system dynamics were analysed during the period of peak heat absorption.

1. Introduction

In 2020, the industrial sector accounted for 30 % of the global energy consumption. Of this energy, 72 % derived from fossil fuels, where natural gas and coal accounted for almost half of the consumption [1]. Solar thermal technologies offer a potential solution for decarbonising this sector and mitigating greenhouse gas emissions [2]. The Solar Heat for Industrial Processes (SHIP) concept includes several temperature ranges of applications (low, medium and high temperature) and different heat transfer fluids such as water or steam, air, or thermal oil. Several examples of applications of the SHIP concept can be found in the literature. For instance, Abedi et al. [3], presented a solar air heater for a desalination system. Bellos et al. [4] studied different solar collectors coupled with an absorption heat transformer for industrial process heating within the temperature range of 80 °C to 160 °C. The collectors included flat plate collectors and evacuated tube collectors. In a separate study, Gebreyohannes et al. [5] optimized a solar-assisted industrial heating and cooling system with maximum temperatures of 160 °C.

However, in industrial processes that require medium and high temperatures, solar concentrating collectors are necessary. Steam is one of the most commonly used heat transfer medium in industrial processes [6]. Concentrating solar collectors can generate steam through either indirect or direct integration. Indirect Steam Generation (ISG) uses a pressurised fluid as the heat transfer medium within the solar collectors. The heat is then transferred to a reboiler through a heat exchanger, where the steam is generated. In Direct Steam Generation (DSG), water is evaporated directly within the solar collector loop and then introduced into a steam drum [6].

In the context of solar process heat, various solar technologies have been implemented depending on the process requirements. For medium-range temperatures (150 −400°C), two mature concentrated solar thermal technologies are commonly deployed: Parabolic Trough Collectors and Linear Fresnel Collectors [7,8]. The potential of the Parabolic Trough collectors to supply heat for processes has been widely studied, modelled and experimentally analysed [9,10,11]. However, there is a lack of research on the potential use of Linear Fresnel collectors for solar process heat supply. Linear Fresnel Collectors have the advantage of a stationary receiver, which eliminates movable joints. Moreover, to emulate a parabolic mirror surface, multiple smaller flat or elastically curved mirrors are used. This allows the receiver to be a separate unit without the need for support from the tracking system, reducing costs

* Corresponding author.
E-mail address: mdavid@iie.upv.es (M.A. David-Hernández).

https://doi.org/10.1016/j.applthermaleng.2024.123418
Received 18 January 2024; Received in revised form 2 May 2024; Accepted 12 May 2024
Available online 14 May 2024

Nomenclature

CSP	Concentrated Solar Power
DSG	Direct Steam Generation
GHI	Global Horizontal Irradiance
ISG	Indirect Steam Generation
SHIP	Solar Heat for Industrial Process

Symbols

b	Standard sensor uncertainty
C_p	Specific heat $(J/(kg{\cdot}K))$
dt	Time period (s)
E	Energy (MJ)
Lvl	Water level (mm)
$\dot{m}$	Mass flow (kg/s)
P	Pressure (bar)
T	Temperature (°C)
U	Uncertainty
$\dot{V}$	Volumetric flow rate (m^3/h)

Subscripts

abs	Absorbed
gen	Generated
inc	Incident
St	Steam
W	Water

and moving parts [12]. However, this comes at the trade-off of lower optical efficiency compared to parabolic troughs [13].

According to a recent report [14], there are currently 20 operational Linear Fresnel collector SHIP systems with published general data. However, information regarding the daily operation of Linear Fresnel collector SHIP plants is scarce. An example of Linear Fresnel technology for process heat generation is the FP7 project InSun [15], which utilises a Linear Fresnel solar field coupled with a containerised balance-of-plant to provide steam to a brick factory. The solar field was divided into two sections: ISG and DSG fields. Monitoring information was reported for each section. References [16] and [17] indicate that the system efficiency does not differ substantially between the two sections. Projects such as FRIENDSHIP [18] and SHIP2FAIR [19] were also developed to demonstrate the techno-economic feasibility and user-friendliness of SHIP technologies in food and agro-industrial processes within the temperature range of 200°C to 300°C.

The RAM Pharma case in the pharmaceutical industry stands is the most well-documented application for monitoring the results of SHIP DSG systems [20,21,22,23]. The SHIP DSG system consists of a Linear Fresnel solar field installed on the rooftop, which is coupled to a steam drum directly connected to the industry's steam network. The SHIP system successfully maintained the pressure of the customer's steam network at the required value throughout a summer day [21]. Frein et al. [22] analysed the performance, drawbacks, uncertainty of measurements, and optimisation of the SHIP solar field in a pharmaceutical plant using a numerical model. Additionally, information on the thermal power delivered to the steam line was presented for both winter and summer days [23]. However, for most of the SHIP plants currently in operation, no further information on their operation or monitoring has been published.

Improved accessibility to operation and performance data measurements is crucial for enhancing the incentive to install SHIP systems. Additionally, it is important to conduct these measurements using accurate instrumentation to monitor performance and heat supply with low uncertainty. This issue is particularly relevant in such installations because they are typically implemented under an energy purchase agreement. In these contracts, the energy company installs the solar systems and sells the energy produced to the customer. Accurate measurement with low uncertainty is essential as the customer only pays for the energy provided and requires a minimum system efficiency. However, these systems often use standard industrial sensors with high uncertainty, such as inaccurate temperature and pressure sensors. The primary reason is the limited scale of these projects, which typically does not justify the expense of high-precision sensors.

In this context, the company Solatom CSP [24] developed a modular Linear Fresnel Collector and installed several SHIP systems in Spain to address this issue. In the framework of the SOLPINVAP project [25], they constructed an experimental SHIP system using this Linear Fresnel Collector technology, capable of operating in both ISG and DSG modes. In the present work, this installation is analysed, specifically focusing on the system operation in ISG mode. Therefore, the following main objectives are established:

- The study of the uncertainty propagation of the standard industrial sensors installed in the system and their influence on the calculation of the energy absorbed and produced by the system.
- The selection of new sensors to calculate the energy absorbed and produced by the steam with low uncertainty.

Furthermore, the study provides measured data from the installation and a detailed insight into the behaviour of control variables under outdoor conditions. This work analyses two days from the experimental campaign: clear-sky and cloudy days. During the operation period, an analysis of the behaviour, control, and performance of the SHIP system is conducted. When compared to existing analyses on SHIP systems that use Linear Fresnel Collectors, this study makes the following novel contributions:

- An uncertainty analysis is conducted using real-time operating data from standard industrial sensors of a SHIP installation with Linear Fresnel Collectors. Based on the results, new sensors were selected and the monitoring system has also been improved, resulting in a 3 % uncertainty in the absorbed and generated heat.
- Real-time measurements have been taken of a SHIP system that operates with Linear Fresnel solar collectors. The system's dynamics have been accurately captured using a high resolution of 10 s, which is crucial for improving the system's control response and performance.
- A comprehensive investigation of the dynamics is presented to improve the understanding of the operational behaviour of such systems.

2. Experimental plant

The system was installed as part of the SOLPINVAP project [25] in an industrial area located in Almassora, Spain (39.958, −0.074). The solar field was designed to generate medium-range temperature heat, from 150°C to 300°C, using modular Linear Fresnel collectors. Although the system can operate in Direct Steam Generation and Indirect Steam generation, this work only focuses on the Indirect Steam Generation (ISG) mode.

The solar array consists of a line of 6 Fresnel collector modules linked in a series, positioned in a north–south orientation with an azimuth angle of 32° northeast (where north is 0°, and south is 180°). The collectors have an inclination angle of 0°. Although these types of collectors typically are not inclined with respect to the ground, they can be mounted on industrial rooftops, adopting the rooftop's inclination angle. On the southern side of the solar field, the Balance-of-Plant has been installed and is connected to the solar field's outlet via a 10m pipeline. Furthermore, there is a 60m return pipeline. Inside the solar field, pressurised water is heated up, and this heat is used to evaporate

water inside the shell of a kettle reboiler (a shell-and-tubes heat exchanger) with a diameter of 600mm and a length of 2.04m. Regarding the steam produced, it is directly released into the atmosphere, with no linkage to an industrial process.

Fig. 1 displays a simplified diagram of the SHIP facility, depicting the key components and instrumentation. The SHIP system is comprised of two circuits: the primary circuit, which functions as the pressurised water close loop, and the secondary circuit, which acts as the steam extraction pipeline. The SHIP system includes three flowmeters: one positioned after the main circulation pump, a steam mass flowmeter located downstream of the extraction valve, and one designated for the makeup water. The solar field is additionally equipped with two temperature sensors at the inlet $(T1)$ and outlet $(T2)$, as well as pressure sensors in the solar field and the kettle reboiler. Furthermore, a pyranometer has been installed to measure the global horizontal irradiance (G in Fig. 1).

2.1. Fresnel collector modules

Solatom CSP [24] has designed and manufactured the Linear Fresnel Collector modules. Each module consists of ten rows of mirrors, which act as primary reflector. These mirrors are equipped with a 1-axis sun-position tracking system that concentrates the incident solar irradiance on the absorber tubes. In addition, the Fresnel module includes a secondary reflector surrounding the absorber tubes that redirects reflected irradiance outside of the focal point into the absorber tubes.

Fig. 2 displays the installation of the Linear Fresnel Collector modules at the SOLPINVAP solar field. The modules are connected in series with a total of 9 absorber tubes with an external diameter of 70mm and a total length of 36m. The absorber tubes are situated 2.97m above the primary reflector. Only six modules were connected in series due to spatial limitations, resulting in increased end losses compared to a typical solar field. Each Fresnel module has an effective reflective aperture area of 26.4m^2. This Fresnel collector module is a first model developed by the company SOLATOM using a trapezoidal secondary reflector. Subsequently, the model was enhanced with an improved tracking system and a Compound Parabolic Concentrator (CPC) secondary reflector.

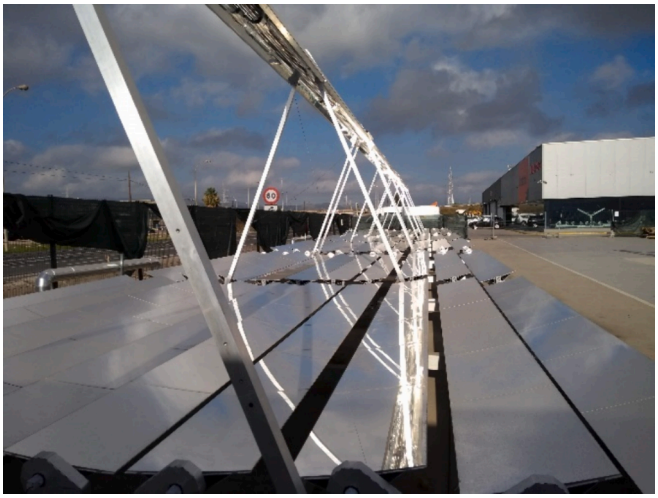

Fig. 2. Linear Fresnel collector modules solar field at the experimental site.

2.2. Control of the SHIP installation

The SHIP system incorporates a PLC located within the skid structure, which records data gathered from the sensors, such as the tank pressure. The system operation is controlled by numerous PID controls that have been programmed in the PLC.

The pump for the primary circuit is activated when the global irradiance is measured to be above 150W/m^2, as determined by the pyranometer. The pump incorporates a frequency control device to adjust the fluid flow rate. The lower limit for the water level inside the kettle

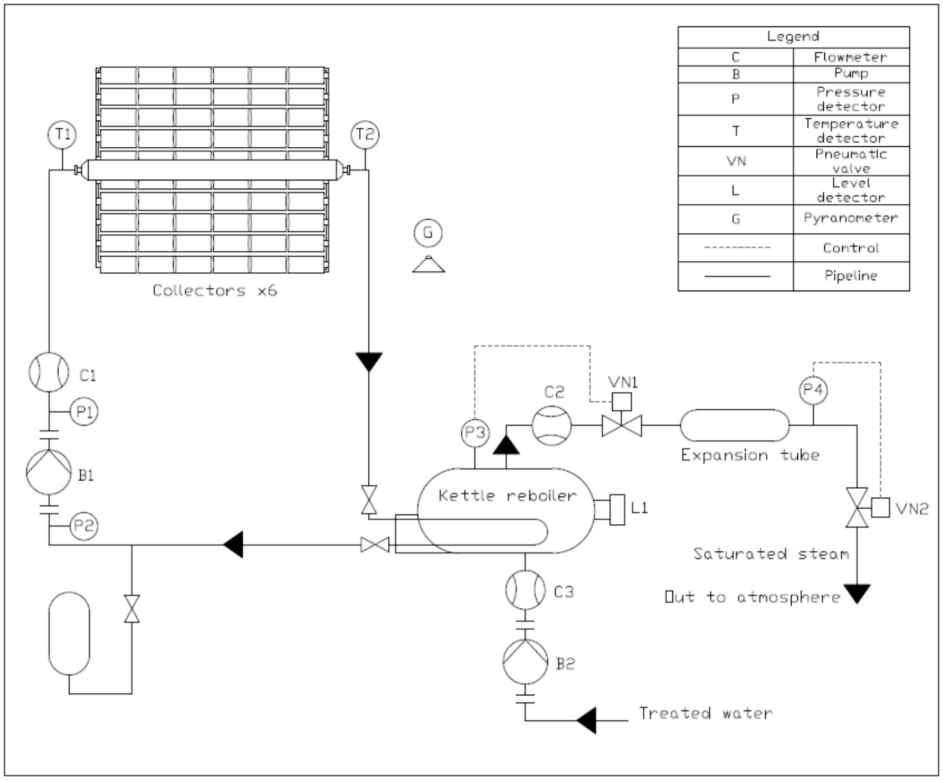

Fig. 1. Simplified diagram of the SOLPINVAP SHIP plant in indirect steam generation mode.

reboiler is $-80mm$, where $0mm$ corresponds to the centre of the kettle reboiler. The liquid level is maintained within a range of minimum and maximum values by treated makeup water, which is introduced at the bottom of the tank when necessary.

Steam extraction is achieved by regulating the opening of two pneumatic valves. The first valve (VN1 in Fig. 1) controls the pressure in the tank. The opening of VN1 is adjusted with a PID control system that operates within predetermined a maximum and minimum pressure parameter. As a result, the pressure within the tank remains consistent with the desired pressure level during steady-state conditions. The second valve (VN2) maintains the pressure inside the expansion tube and by adjusting its opening, the pressure in the expansion tube is regulated, thereby simulating the process pressure.

3. Uncertainty analysis of real measurements

The performance of the SHIP system is contingent upon the amount of energy absorbed by the collectors, the accumulated energy, and the extracted heat. While these quantities cannot be directly measured, they can be derived from physical variables that can be measured. However, the uncertainty in each measurement has an impact on the level of uncertainty in the final energy output.

3.1. Energy produced by the system

The energies defined by equations (1) to (3) are integrated values over the analysed time period. Equation (1) represents the absorbed energy in the solar field (E_{abs}), thus the useful energy, while equation (2) demonstrates the generated energy (E_{gen}) based on the measured mass flow rate of extracted steam ($\dot{m}_{st}$) and its specific enthalpy, which is dependent on the pressure measured inside the kettle reboiler ($h_{st} = f(P_{kettle})$). The energy supplied by the makeup water (E_w) is given by equation (3), where T_w is the measured temperature of the makeup water, $\dot{m}_w$ represent the makeup water mass flow rate and $C_{p,w}$ is its specific heat.

$$E_{abs} = \int \dot{m} \cdot C_p \cdot (T_2 - T_1) \cdot dt \tag{1}$$

$$E_{gen} = \int \dot{m}_{st} \cdot h_{st} \cdot dt \tag{2}$$

$$E_w = \int \dot{m}_w \cdot C_{p,w} \cdot T_w \cdot dt \tag{3}$$

As it can be seen from the previous equations, the calculation of the absorbed energy is directly influenced by the mass flow rate through the primary circuit ($\dot{m}$) and the inlet (T_1) and outlet (T_2) temperatures of the solar field. The temperature sensors are positioned at the inlet and outlet side of the collectors, as depicted in Fig. 1. Measurement of temperatures is essential because the uncertainty in the calculation of the absorbed energy increases as the temperature difference decreases.

The energy and mass balances of the system are expressed in the equations (4)-(5):

$$E_{abs} + E_w = \Delta U + E_{gen} + E_{loss} \tag{4}$$

$$\Delta U = M_2 \cdot u_2(P_2, v_2) - M_1 \cdot u_1(P_1, v_1) \tag{5}$$

Where the specific internal energy u of the fluid is a function of the kettle reboiler pressure P and its specific volume v of the fluid, and ΔU represents the total internal energy change of the tank. The two-phase fluid's mass at the beginning of the sample (M_1) can be determined by considering the water level, tank geometry and fluid properties at saturated state. Furthermore, M_2 is the sum of the initial fluid's mass and the difference between the inlet and outlet mass flows is represented by $M_2 = M_1 + (M_{in} - M_{out})$. Equations (1)-(3) and (4)-(5) were integrated, along with their corresponding uncertainties. The energy lost component has been calculated using the difference of the integrated energies in Equation (4).

3.2. Initial and new sensors

During the construction of the SHIP plant, a set of sensors is typically installed in the solar field to control and monitor the installation's performance based on the measured values. However, as pointed out by Hofer [26], the standard industrial sensors and equipment for operation and control usually have considerable high uncertainties. Hence, the readings might not be appropriate for performing accurate energy balances. For this reason, new instrumentation was added to increase the measurement's accuracy and reliability. Three sensors were identified as critical due to their significance in calculating the absorbed and generated heat:

- The temperature at the inlet and outlet of the solar collectors has a direct effect on the calculated energy within the solar field.
- The absolute pressure in the kettle reboiler affects the specific enthalpy of the extracted steam.
- An acquisition system has been installed with a datalogger to replace the previously installed PLC. This new system affects the precision and acquisition time of all the measurements.

The initial instrumentation is detailed in Tables 1-4, together with the new instrumentation selected to reduce the uncertainty in the measurements. The standard uncertainties provided by the manufacturers are shown in these tables. The standard uncertainty of both flow meters is shown in Table 4. The confidence interval used for each sensor is shown in each table (2σ or 3σ), according to their corresponding datasheets.

When comparing the specifications of the initial sensors and equipment with the proposed new ones, it is evident that there is a significant improvement in the measurement uncertainty. The following section will detail the effects of this reduction in uncertainty through an uncertainty propagation analysis and how it affects in the system's performance.

3.3. Uncertainty propagation

The uncertainty propagation analysis was conducted by performing an energy and mass balance of the SHIP system to assess the reliability of the measurements and the operation of the solar field. The uncertainty analysis was conducted using the methodology described by Coleman and Steele in [27], which is commonly used in engineering.

In order to study the system's performance, several simplifications were made, such as:

- The kettle reboiler has been simplified by considering it as a horizontal cylinder.
- Throughout the study period, the water in the tank was assumed to be in thermodynamic equilibrium as two-phase fluid. Therefore, the liquid and vapour parts inside the tank are considered to have the properties of saturated liquid water and saturated steam at the working pressure, respectively. This study analyses the SHIP system

Table 1
Type and standard uncertainty of Initial and new temperature sensors.

Initial sensor		New sensor	
Type	**Standard Uncertainty (2σ)**	**Type**	**Standard Uncertainty (2σ)**
RTD PT100 class A	$\pm(0.15 + 0.002 \cdot \lvert T \rvert)$	RTD PT100 class 1/10	$\pm(0.03 + 0.0005 \cdot \lvert T \rvert)$

Table 2
Technical characteristics of the initial and new pressure transmitter.

Source	Initial sensor (2σ)	New sensor ($3\ \sigma$)	Unit
Precision	0.5	0.065	% of measurement
Repeatability	0.05	Not provided	Of range
Hysteresis	0.1	Not provided	% of range
Stability	Not provided	0.2	% of range
Type	Piezoresistive	Digital sensor	–

Table 3
Standard uncertainty of the PLC and datalogger.

	Function	Range	Standard Uncertainty
PLC	DC Current	4–20 mA	0.4 % (2σ)
Datalogger	DC Current	4–20 mA	0.05 % of reading + 0.005 % of range ($3\ \sigma$)
	RTD	-200C to 600 °C	0.06 °C ($3\ \sigma$)

Table 4
Type and standard uncertainty of the water and steam flow meter.

	Flow Meter (2σ)	
Source	Water	Steam
Measurement	0.75%$\dot{V}$	2%$\dot{m}$
Type	Vortex	Target

during a working period where the tank's behaviour is comparable to steady-state, making the assumption of equilibrium reasonable.
- The control volume for assessing the system performance is the complete SHIP system.

An uncertainty propagation analysis was conducted using measurements taken on June 11th, 2022. This date was chosen as it represents a typical day for steam production. The solar collectors achieved a maximum temperature difference of 7.2K. The global horizontal irradiance for this day was consistent with a typical clear-sky day and peaked at 862W/m^2 during solar noon, as shown in Fig. 3. Cloudy conditions were observed between 6 and 10 h solar time. At 17:30 solar time, a sharp decline in GHI is observed in the measurements presented in Fig. 3. The decline in irradiation is caused by a shadow from a nearby structure being cast upon the pyranometer. This trend is observed in all the measurements. However, this does not affect the system's performance, as it occurs at the end of the day. The water levels were set to a maximum of 35 and a minimum of 5 mm, as depicted in Fig. 3.

Steam extraction was initiated by the control at a pressure set point of 6bar_a with a hysteresis of 1bar, as shown in Fig. 4. Steam mass flow was registered as soon as the tank reached the set pressure. The pressure within the expansion tube was also maintained to replicate a heat requirement of steam at approximately 135°C.

On June 11th, 2022, the maximum registered absorbed heat was of 50.6kW_{th}. Fig. 5 displays the instantaneous normalised absorbed thermal power in the collector field. The thermal power was calculated using Equation (1). The shape of the curve is comparable to that reported in Ref. [16] for a Linear Fresnel collector ISG solar field, where the instantaneous normalised thermal power of the ISG solar field is also presented.

In Fig. 5, the power drops to 10 % and then from 65 % to 55 % when clouds covered the solar field. It is important to note that the peak power does not occur at solar noon because of the azimuth angle of the collectors.

To conduct the uncertainty propagation analysis, a time frame was selected during which the solar field's temperatures and kettle reboiler pressure remained almost constant. A 28-minute period between 11:33 and 12:01 was chosen, consisting of 168 continuous measurements. The measurements were recorded using a datalogger with a 10-second time interval, while the PLC recorded measurements at a 60-second interval. It is important to note that using discrete measurements, such as a 60-second interval, may overlook the impact of instantaneous events, such as a cloud passing over the collector field between readings. During steady-state, between the 60-second and 10-second the absorbed energy values exhibit negligible differences. However, during a transient period, the divergence is approximately 4 %.

The uncertainty propagation analysis measurements were selected during a time period when the initial and end points had similar pressure and mass, ensuring a steady state period. Fig. 6 a) and b) display the measurements for the analysed period. Fig. 6 a) demonstrates that the initial and final water levels remained at a similar value. Furthermore, the temperatures of the solar field and the kettle reboiler remained stable. Fig. 6 b) shows that when makeup water is introduced into the tank, the steam mass flow rate decreases, leading to a reduction in pressure inside the expansion tube. This phenomenon is further described in section 4. However, after this transient period, the steam mass flow increases until it reaches a steady flow. Therefore, it can be inferred from Fig. 6 that the two-phase fluid inside the tank is saturated,

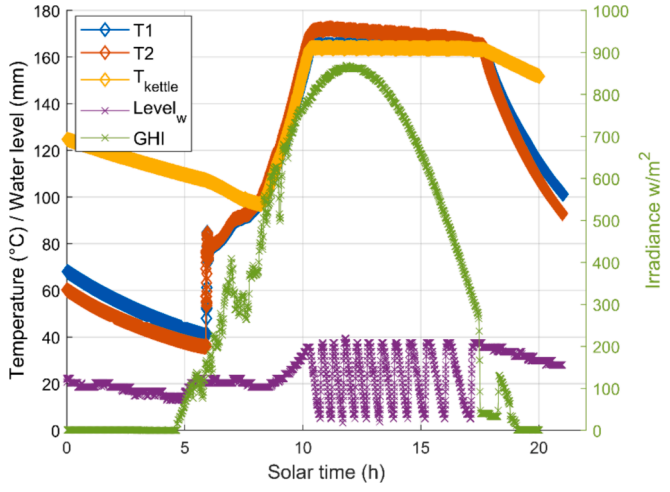

Fig. 3. Measurements taken on-site of the solar field and kettle reboiler temperatures, water level in the tank, and the global irradiance on June 11th, 2022.

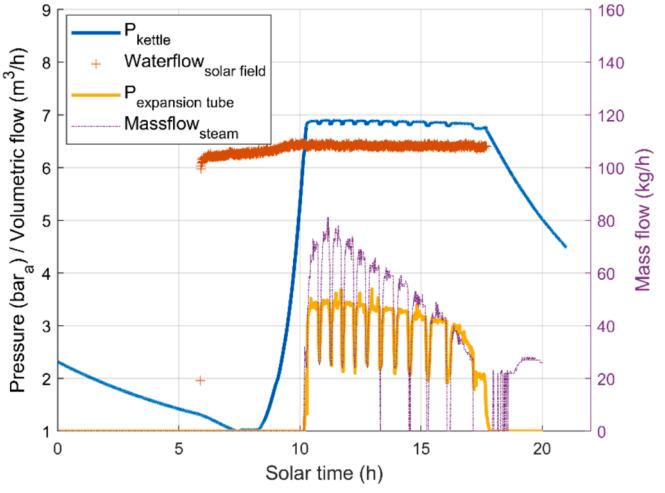

Fig. 4. Measurements taken on-site of the pressure of the kettle reboiler and expansion tube, the volumetric flow of water in the solar field, and the mass flow of extracted steam on June 11th, 2022.

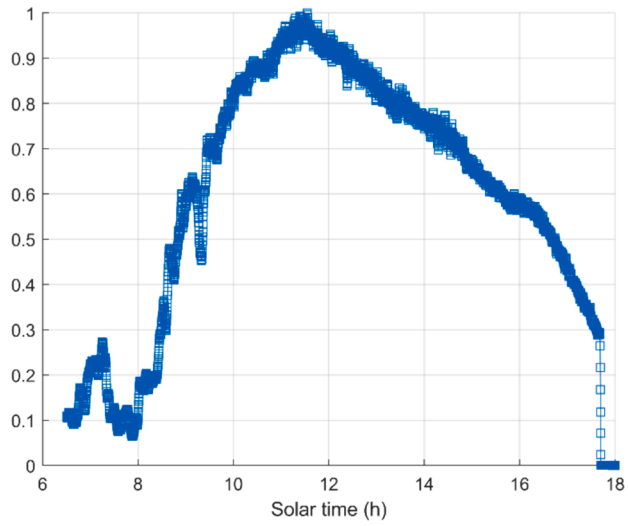

Fig. 5. Instantaneous normalized thermal power on June 11th, 2022.

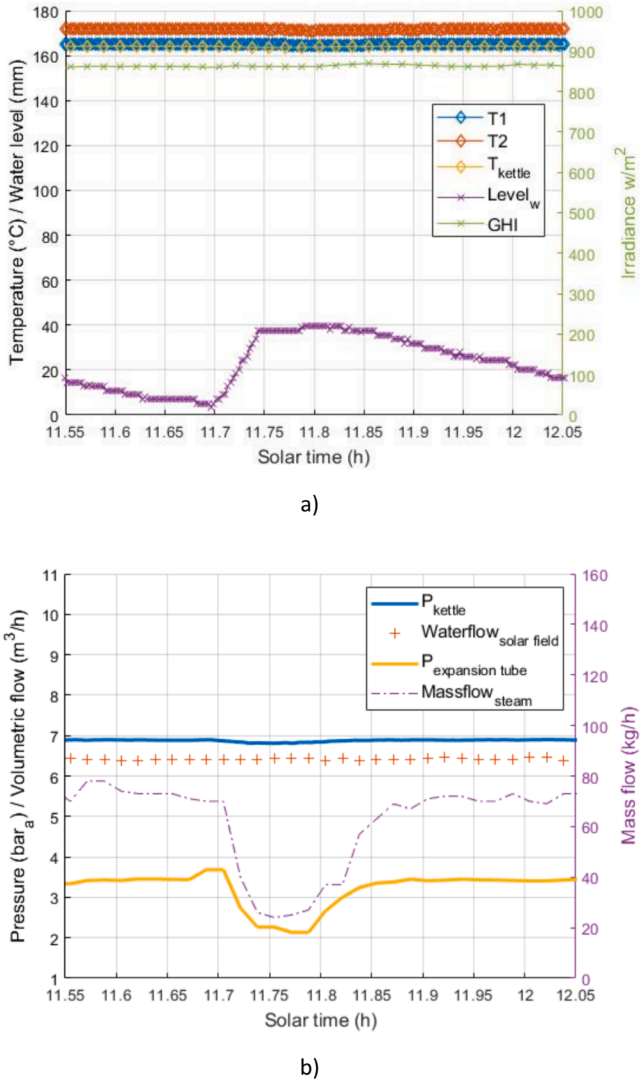

Fig. 6. Solar field's measured variables: a) Inlet (T1) and outlet (T2) solar field temperatures, tank temperature, water level, irradiance; b) Pressure on the kettle reboiler and expansion tube, water volume flow and steam mass flow for the uncertainty analysis.

and that the change in internal energy in Equation (4) is negligible ($\Delta U \approx 0$).

To calculate the expanded uncertainty of each measurement, the standard uncertainty values of each sensor were reduced to a 1σ confidence level and then expanded to a 2σ confidence level, taking into account all the uncertainties associated with the specific measurement. For instance, the components that interact in the temperature measurements are the RTDs and the datalogger. The expanded uncertainty with a confidence level of 2σ was calculated by using Equation (6). Where b represents the error with a confidence level of 1σ, and U_x represents the expanded uncertainty with a confidence level of 2σ.

$$U_x = 2 \cdot \sqrt{b_1^2 + b_2^2 + \cdots + b_n^2} \tag{6}$$

The calculated expanded uncertainties presented in Table 5 are the average values measured for each variable. The uncertainty of the temperature measurements decreased from ±0.57 to ±0.12, resulting in a 79 % decrease in the expanded uncertainty due to the implementation of the new sensors and equipment. Furthermore, there was also a reduction regarding the kettle reboiler pressure measurement.

Table 6 presents the average heat absorbed and generated during the studied period, along with their respective uncertainties. The newly installed sensors introduce an uncertainty of approximately 3 % in the absorbed heat, which is within the range of uncertainty for process heat collectors when using invasive measurement sensors as reported in Ref. [26]. The uncertainty of the generated heat is also 3.3 %. When using the default sensors and their corresponding measurements during the same time period, the absorbed heat uncertainty is 12.3 %. Based on the results presented in Table 6, it can be concluded that the absorbed heat of 46.6kW is a more accurate value than the initial sensors calculation of 51.4kW, taking into account the uncertainties introduced by both the new and the initial sensors, as demonstrated in Fig. 7. Thus, the uncertainty in the absorbed heat was reduced by 76.8 %.

The SHIP plant measurements taken with the new sensors were used to perform an energy and mass balance calculation of the absorbed, generated, and lost energy of the SHIP system, alongside their related uncertainties. The resulting values are presented in Table 7. Over the examined period, the SHIP system lost an estimated $1.73 \pm 0.76kWh$ of energy to the environment, resulting in a mean heat loss of $3.7 \pm 1.6kW$. If the SHIP system's lost energy was estimated using the default instrumentation, the mean heat loss would be $8.5 \pm 6.4kW$.

4. System operation and monitoring results

This section examines the performance of the Fresnel SHIP system on two distinct days, one clear and one cloudy, selected as representative of summer conditions. This data was selected from a measurement campaign conducted during the summer of 2022 carried out to demonstrate the significance of precise monitoring and gain insight into the system's behaviour.

Table 5
Sensor mean expanded uncertainty of the initial and new instrumentation with a 95 % of confidence.

Magnitude	Sensor	Uncertainty initial instrumentation	Uncertainty new instrumentation	Units
Temperature	T_1	±0.567	±0.123	K
	T_2	±0.578	±0.127	K
Pressure	P_{kettle}	±0.048	±0.027	bar
	P_1	±0.118	±0.074	bar
Flow	$\dot{V}_w$	±0.054	±0.054	m^3/h
	$\dot{m}_{st}$	±1.3	±1.3	kg/h
Water Level	lvl_{kettle}	±4.08	±4	mm

Table 6
Mean absorbed and generated thermal power before and after the new instrumentation.

Magnitude	Initial instrumentation		New instrumentation	
	Value (kW)	Uncertainty (kW)	Value (kW)	Uncertainty (kW)
Mean absorbed heat	51.40	±6.31(12.3%)	46.59	±1.32(3%)
Mean generated heat	46.56	±1.53(3.3%)	46.53	±1.53(3.3%)

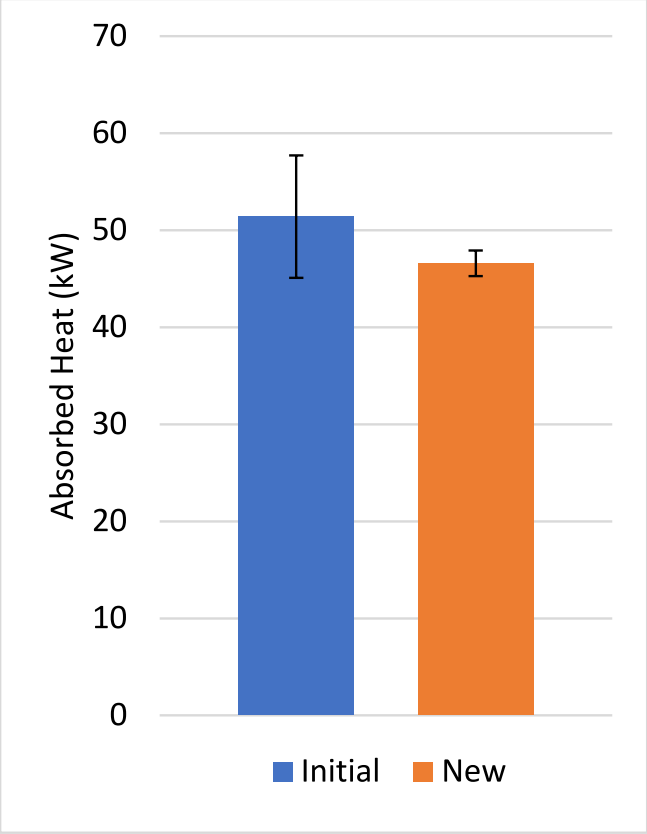

Fig. 7. Mean absorbed thermal power with the initial and new sensors and their corresponding uncertainty.

Table 7
Total energy before and after the new instrumentation.

Magnitude	Initial instrumentation		New instrumentation	
	Value (kWh)	Uncertainty (kWh)	Value (kWh)	Uncertainty (kWh)
Absorbed energy	24	±3(12.3%)	21.61	±0.61(2.8%)
Generated energy	21.72	±0.46(2.1%)	21.58	±0.46(2.1)
Feed water energy	1.7	±0.08(5%)	1.7	±0.08(5%)
Lost energy	4	±3(75.2%)	1.73	±0.76(43.8%)

4.1. Operation on day 1: Clear-sky day

The first analysed day was May 31st, 2022 (day 1), with normal steam production conditions. The pressure set point for the kettle reboiler was set at $4bar_a$, with a hysteresis of $0.3bar$, and the water level was maintained between the maximum and minimum limits of 20 mm and 5 mm, respectively. The operation on day 1 is depicted in Fig. 8 and Fig. 9. Fig. 9 shows that the pressure within the expansion tube was maintained above $3bar_a$, for the purpose of replicating industrial processes characterised by saturated steam demand at 133.5°C. On this day, a clear-sky GHI profile was observed, shown in Fig. 8, with a GHI of $860.7W/m^2$ at solar noon.

On day 1, the peak heat absorption occurred between 10 am and 12 pm solar time, as displayed in Fig. 8. From 12 pm onwards, the temperature T2 at the solar field outlet decreased at a consistent rate until the circulation pump was switched off. The largest temperature difference measured in the solar field reached $5.9K$, with $41.74kW$ and $49.46kW$ of maximum heat absorption and extraction, respectively. In addition, the average ambient temperature throughout the day was 26.24°C and the maximum steam mass flow rate was $65kg/h$.

Around 6 am, the main circulation pump was switched on, and subsequently, a drop in the tank's pressure and temperature was observed. This phenomenon happened because the fluid exiting the solar field was colder than the water inside the tank. As a result, the primary circuit's water absorbed heat from the tank via the heat exchanger.

In Fig. 9 is observed that, after the activation of the pump, a transient state in the flow occurs due to the presence of air in the pressurized water. However, a valve purges the air as the water temperature increases. This fluctuation is approximately 5 % and does not significantly affect the overall performance. In addition, a transient oscillation stage was observed in the temperatures of the solar field for 22 min until they stabilised. Additionally, it took the system 1 h and 16 min to initiate the pressurisation of the kettle reboiler. On day 1, the pressurisation transient period was 1 h and 53 min. Therefore, the SHIP system required 3 h and 29 min from pump activation to the kettle reboiler reaching its operating condition. Once the kettle reboiler reached the pressure set point, the Fresnel SHIP system operated under stable conditions for 8 h and 24 min, which accounts for 35 % of a full day. Throughout this time, the system maintained a consistent tank pressure.

Throughout the course of the operation, the makeup water pump completed 24 filling cycles, and the kettle reboiler maintained a consistent pressure level of approximately $4.3bar_a$. However, the pressure in the tank and in the expansion tube dropped when cold water was introduced into the tank. This phenomenon is analysed in further detail in Fig. 10 and Fig. 11, which display the solar field's measured variables between 11:00 and 11:54 solar time. When the water level fell below the minimum threshold, the makeup water pump was activated, and water at 50°C was introduced into the kettle reboiler.

Fig. 10 depicts the pressure of the tank and expansion tube, alongside

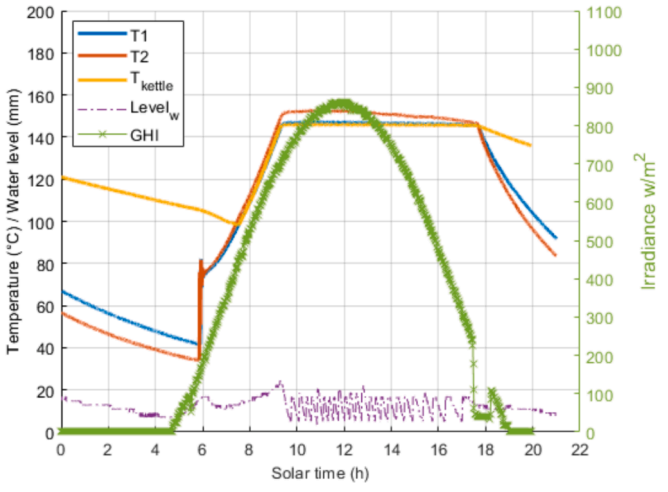

Fig. 8. Inlet (T1) and outlet (T2) solar field temperature, kettle reboiler temperature, water level, and GHI on day 1.

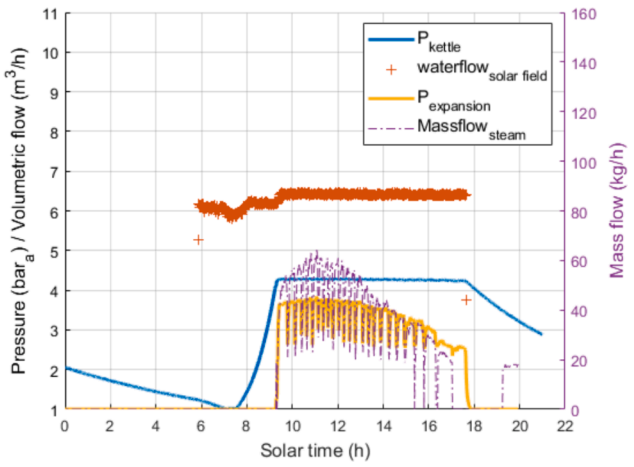

Fig. 9. Kettle reboiler and expansion tube pressure, water volumetric flow rate, and steam mass flow rate on day 1.

the opening percentage of pneumatic valves for extraction V1 and outlet V2. The steam mass flow decreased gradually in proportion to the increase in water level. This is due to the change in fluid mass caused by colder water, resulting in a reduction of the fluid's total energy of the fluid and a consequent decrease in the tank's pressure.

The extraction valve, V1, responded to the pressure drop of the tank and reduced its opening by 10 % leading to a decrease of steam flow, a pressure drop within the expansion tube, and closure of the outlet valve, V2. In the expansion tube, there was a pressure decrease of 0.74*bar*, whereas in the kettle reboiler there was a pressure drop of 0.03*bar*, and the steam mass flow rate changed from 60*kg*/*h* to 30*kg*/*h*, as shown in Fig. 10. The expansion tube's pressure is highly sensitive to upstream pressure changes; therefore, a constant steam mass flow was maintained for a brief period of 9 min.

The pressure drop across the kettle reboiler resulted in a decrease in its internal temperature, which subsequently led to a reduction in the inlet water temperature of the solar field, as depicted in Fig. 11. However, despite changes in the tank's pressure, a constant temperature difference was still achieved in the solar field.

Table 8 shows the results of the absorbed, and generated energy during the operating period on day 1.

4.2. Operation on day 2: Cloudy day

A cloudy day was selected as day 2, corresponding to June 12th, 2022. On this day, the pressure set point for the kettle reboiler was stablished at 6bar_a with a hysteresis of 1*bar*. The minimum and maximum water level limits were set at 5 mm and 35 mm, respectively. Furthermore, the kettle reboiler pressure was recorded at 1.8bar_a prior to activation of the main circulation pump. The measurements are displayed in Fig. 12 and Fig. 13.

The period of the day that experiences the most absorbed heat occurs between 10 am to 12 pm solar time, resulting in a temperature

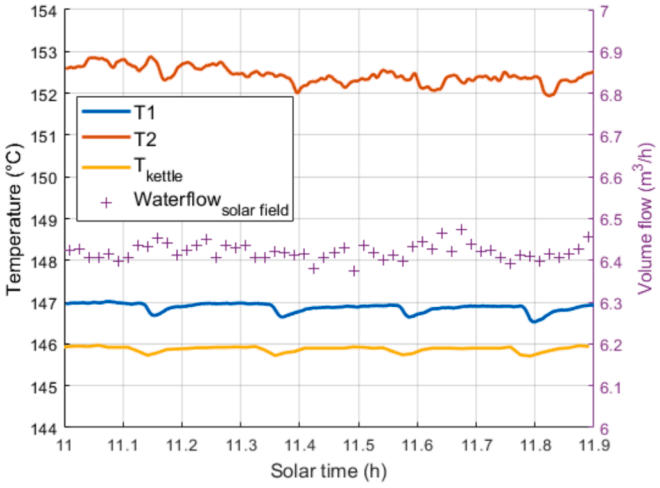

Fig. 11. Detailed view of the inlet (T1) and outlet (T2) solar field temperature, kettle reboiler temperature, and solar field's water volume flow during the analysed period on day 1.

Table 8
Total absorbed and generated energy throughout the operating period on day 1.

Magnitude	Value
Absorbed energy	242.25 ± 9.8 (4 %) kWh
Generated energy	233.98 ± 8.1 (3.4 %) kWh

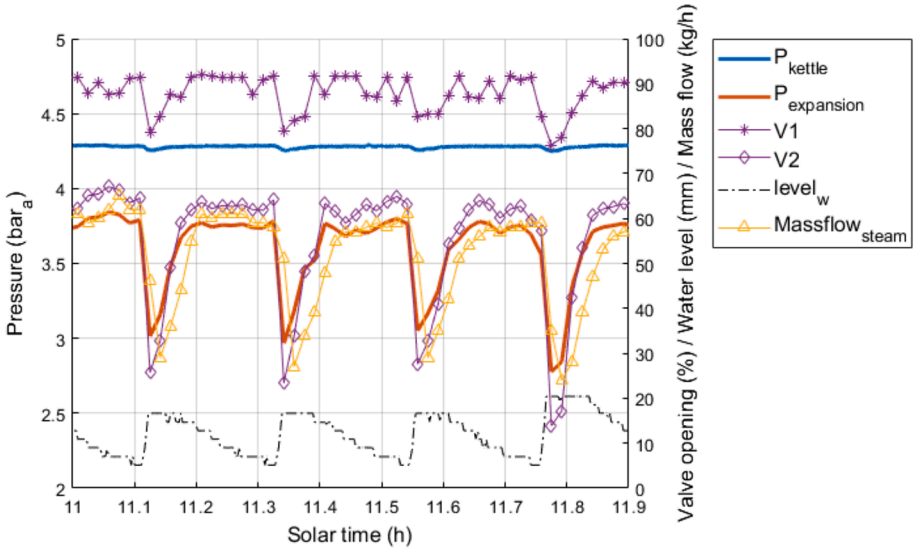

Fig. 10. Detailed view of the kettle reboiler and expansion tube pressure, extraction (V1) and outlet (V2) pneumatic valve opening (%), water level, and steam mass flow during the analysed period on day 1.

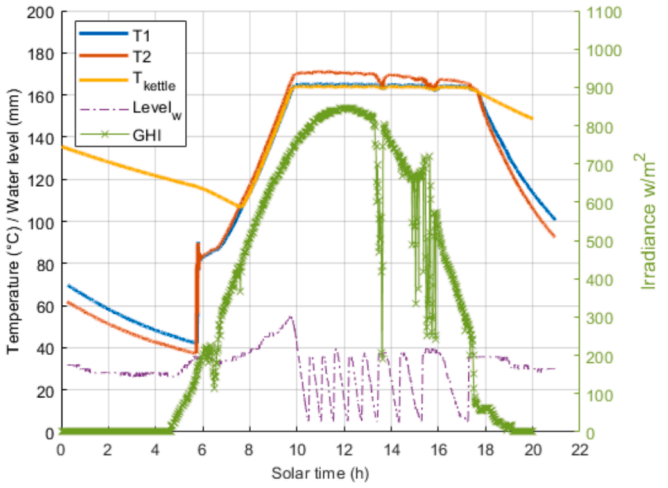

Fig. 12. Inlet (T1) and outlet (T2) solar field temperature, kettle reboiler temperature, water level, and GHI on day 2.

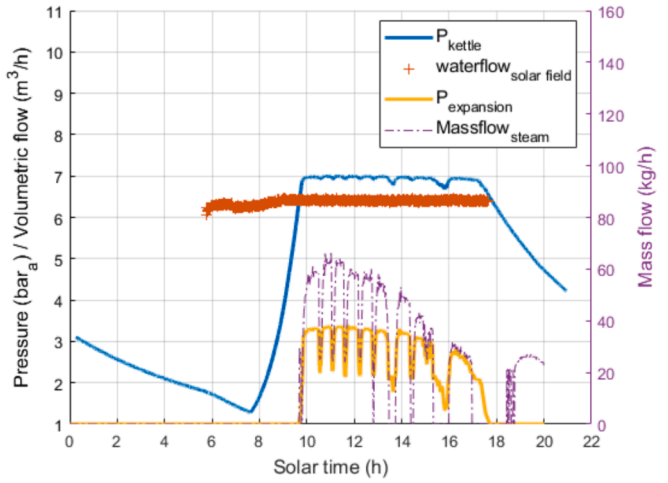

Fig. 13. Kettle reboiler and expansion tube pressure, water volumetric flow rate, and steam mass flow rate on day 2.

difference of up to 6K. The maximum absorbed and generated heat were recorded at 42.63kW and 51.41kW, respectively. Furthermore, the maximum recorded steam mass flow was 67kg/h, with an average ambient temperature of 32.3°C throughout the day.

The initial fluctuation in the solar field's temperatures, following activation of the circulation pump, lasted 17 min until stability was achieved. Fig. 12 depicts GHI measurements, where a cloud period of 40 min was observed, resulting in a lower rate of temperature increase compared to clear-sky conditions. Afterwards, the SHIP system took 1 h and 52 min to initiate kettle reboiler pressurisation. The tank pressure exceeded atmospheric pressure by 0.3bar at the start of the pressure rise, as observed in Fig. 13. On day 2, the system required a transient pressurisation period of 2 h and 9 min to reach operating conditions. It took 3 h and 35 min to reach operating conditions from the time when the pump was switched on until the kettle reboiler operating pressure was achieved.

The system operated smoothly for 3 h and 24 min before a second cloud was registered. At 13:10, the cloud covered the solar collectors and persisted for a duration of 33 min. Consequently, the outlet temperature of the solar field decreased to a minimum of 163.45°C, leading to a decline of 0.2bar in the kettle reboiler. Nevertheless, the kettle reboiler pressure recovered to its operating condition within a period of 17 min and remained consistent for a further hour and 19 min. At 14:46, a third transient cloud was recorded, lasting for 1 h and 11 min. This caused the tank pressure to decrease by 0.27bar. After the cloud cleared, the tank pressure returned to its operating condition within 19 min. The system operated for 1 h and 33 min before the pump was shut down. Overall, the SHIP system worked under operating conditions for 7 h and 50 min, equivalent to 33 % of a full day.

On both day 1 and day 2, the time required to achieve the operational condition was comparable. This similarity arises from the fact that on day 1, the tank initiated from 1bar_a, while on day 2, a cloud cast a shadow over the solar field, consequently delaying the heating of the kettle reboiler.

As depicted in Fig. 9, following the system shutdown, there was a significant reduction in pressure in the kettle reboiler, occurring between 18:00 and 19:00, with a pressure drop of 0.46 bar. Fig. 13 further illustrates a pressure decrease of 0.82 bar during the same interval. This indicates the substantial heat loss of the system to the ambient, as calculated in section 3. Nevertheless, despite the significant heat loss, the kettle reboiler initiated on day 2 from a pressurised condition.

On day 2, the maximum limit for water level control limit was raised by 15 mm above the limit for day 1. The makeup water pump completed 9 filling cycles, as illustrated in Fig. 12. Meanwhile, the kettle reboiler pressure was maintained at a constant pressure level of 6.9bar_a throughout the operating period. Fig. 14 and Fig. 15 depict the solar field's measured variables analysed from 11:00 to 11:54. Fig. 14 demonstrates the impact of the introduction cold water. However, a constant steam mass flow rate is maintained for a duration of 21 min due to the rise in the water level gap limit. Variations in the pressure of the kettle reboiler affect the steam flow rate and the pressure within the expansion tube. In Fig. 10, there are four makeup water cycles throughout the analysed period, whereas there are only 2 makeup water cycles in Fig. 14 during the same period. By adjusting the liquid level control limits, the number of makeup water cycles decreases during operation, allowing for a constant steam flow to be extracted at a constant pressure over a longer period.

Over the course of the analysis, there was a 7 % decrease in the extraction valve opening and a 60 % reduction in the outlet valve opening. The kettle reboiler pressure fell by 0.08bar, while the pressure in the expansion tube dropped to 1bar. Fig. 15 shows that there was a constant temperature difference in the solar field during the analysis, despite the introduction of low-temperature water into the kettle reboiler, resulting in a decrease in the solar field inlet temperature. Table 9 shows the results for the operating period on day 2.

Despite a lower total absorbed energy on day 2 compared to day 1, the solar field and SHIP system demonstrated improved performance on day 2.

5. Conclusions

Accurate determination of the absorbed and generated heat is essential in evaluating the performance and heat output of a heat production system, particularly when supplying heat to a customer while maintaining reasonable efficiency. However, conventional Solar Heat for Industrial Processes (SHIP) systems often use standard sensors and equipment that are low cost but have high uncertainty, leading to potential inaccuracies in the evaluation of system performance. To emphasise the significance of precise monitoring, an uncertainty propagation analysis was conducted on the monitoring system of an actual SHIP system that produces steam using Linear Fresnel collectors in ISG mode. The analysis revealed that the standard industrial sensors introduced significant uncertainty when calculating the absorbed heat. New sensors and equipment were installed to enhance accuracy, successfully reducing the uncertainty in the absorbed heat from over 10 % to below 5 %, even with small temperature differences in the solar field.

Furthermore, an operational analysis was conducted on the SHIP system to demonstrate its behaviour. During an experimental campaign in the summer of 2022, insights were gained from two measured days:

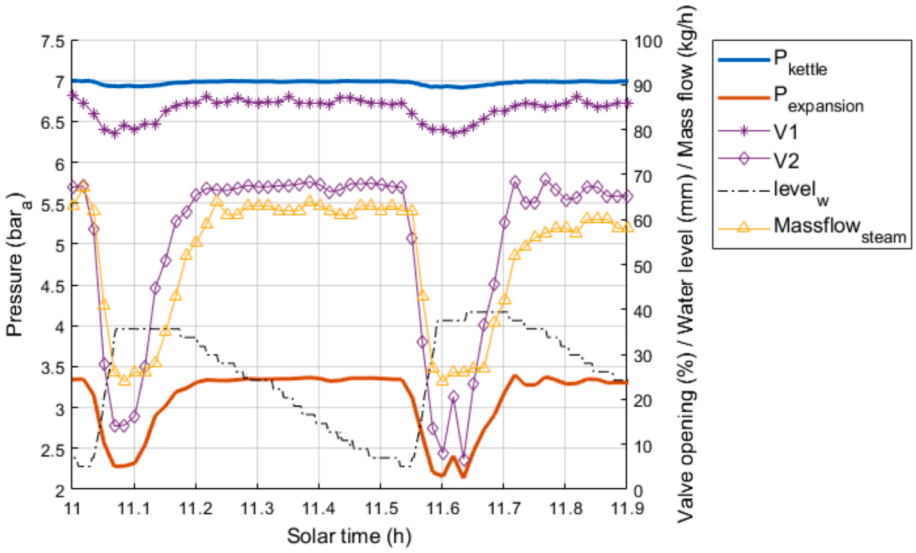

Fig. 14. Detailed view of the kettle reboiler and expansion tube pressure, extraction (V1) and outlet (V2) pneumatic valve opening (%), water level, and steam mass flow during the analysed period on day 2.

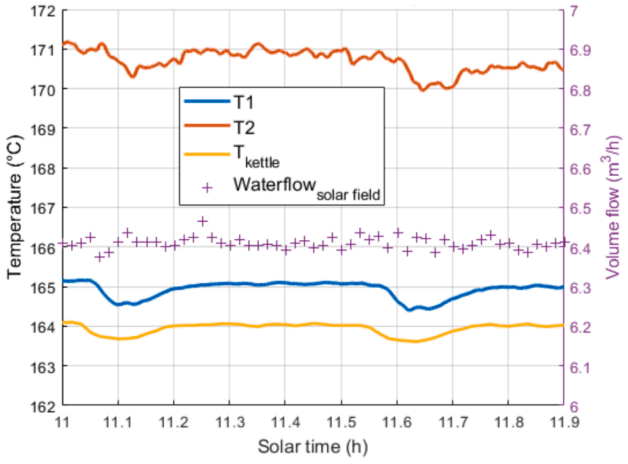

Fig. 15. Detailed view of the measured variables during the analysed period on day 2. Inlet (T1) and outlet (T2) solar field temperature, kettle reboiler temperature, and solar field's water volume flow.

Table 9
Absorbed and generated energy throughout the operating period in day 2.

Magnitude	Value
Absorbed energy	226.35 ± 9.9 (4.4 %) kWh
Generated energy	206.98 ± 7.8 (3.7 %) kWh

one with clear-sky conditions and the other with clouds. The results show that the time taken to reach the operating pressure was comparable on both days, despite differences in pressure setpoints and irradiance conditions. On the cloudy day, the system returned to the setpoint pressure under 20 min after a transient cloud passed over the collector field. A wider hysteresis in the control band of the kettle reboiler water level's makeup water contributed to more consistent and stable steam mass flow for extended periods. Moreover, the generated energy on the cloudy day was 11.5 % lower than on the clear-sky day.

Reducing the sampling rate from 60 to 10 s improved the understanding of the system dynamics and variations in operational parameters under changing weather conditions. The calculation of total energy showed no significant difference in the calculation of total energy between the 60- and 10-second sampling rates during steady-state conditions. However, during transient states, the difference increased due to rapid system changes.

These analyses demonstrate the significance of implementing a precise monitoring system with low uncertainty and short acquisition time. This is essential for Energy Service Companies (ESCOs) to prevent financial losses.

The integration of solar process heat to decarbonise the manufacturing processes poses a challenge for industries due to the limitation of heat for 1/3 of the day. Therefore, there is still room for improvement in solar heat for industrial process systems. This can be achieved by exploring the integration of thermal energy storage and hybridisation with other technologies, such as heat pumps. It is also important to note that this study only performed measurements during the summer and in ISG mode to accurately measure the useful heat from the collectors and the effect of the control on the system's behaviour. Furthermore, the studied system is relatively small compared to currently operating SHIP systems. However, the temperature difference obtained in the collector row is representative of this type of systems.

CRediT authorship contribution statement

Marco A. David-Hernández: Writing – review & editing, Writing – original draft, Validation, Software, Methodology, Investigation, Formal analysis, Data curation, Conceptualization. **Antonio Cazorla-Marín:** Writing – review & editing, Visualization, Supervision, Methodology. **José Gonzálvez-Maciá:** Supervision, Resources, Project administration, Funding acquisition. **Jorge Payá-Herrero:** Writing – review & editing, Supervision. **Miguel Frasquet:** Writing – review & editing, Resources.

Declaration of competing interest

The authors declare that they have no known competing financial interests or personal relationships that could have appeared to influence the work reported in this paper.

Data availability

Data will be made available on request.

Acknowledgements

The authors gratefully acknowledge the company Solatom CSP, for the information and operational data from the SHIP facility, and for the technical support, specially to Juan Martínez and Carlo Terruzzi. This work was partially supported by the Research and Development Aid Program (PAID-01-20) of the Universitat Politècnica de València for receiving the Research Fellowship FPI-UPV-2020. This publication has been carried out in the framework of the project "DECARBONIZACIÓN DE EDIFICIOS E INDUSTRIAS CON SISTEMAS HÍBRIDOS DE BOMBA DE CALOR", founded by the Spanish "Ministerio de Ciencia e Innovación (MICIN)" with code number PID2020-115665RB-I00. The project was also partially funded by the R&D project SolarSteam4IND (TED2021-130614A-I00), funded by MICIN/AEI/10.13039/501100011033/ and by the European Union NextGeneration EU/PRTR 2021 call.

Appendix A. Uncertainty calculation

A.1. Expanded uncertainty of a measurement

The methodology followed to calculate the uncertainty related to variables of interest is further detailed with the following examples:

Example 1. The temperature in the outlet of the solar field is 171°C and the standard uncertainty related to the measuring sensor is $0.03 + 0.0005 \cdot |T|$. The standard uncertainty of the datalogger for a RTD temperature measurement is 0.06°C. Thus, the uncertainty with a 1σ confidence level for each component would be as follows:

$$b_T = \frac{0.03 + 0.0005 \cdot |171|}{2} = 0.057 \tag{A.1}$$

$$b_{DL} = \frac{0.06}{3} = 0.02 \tag{A.2}$$

The expanded uncertainty with a 2σ confidence level is calculated as follows:

$$U_T = 2 \cdot \sqrt{b_T^2 + b_{DL}^2} = 0.122 \tag{A.3}$$

Therefore, the uncertainty of that temperature measurement is 171 ± 0.122°C°C.

A.2. Heat uncertainty

Example 2. In the solar collector field, there is a temperature of 165.19 ± 0.12°C at the inlet and 171.88 ± 0.13°C at the outlet. Additionally, there is a water mass flow of $1.61 \pm 0.01 kg/s$, and considering the specific heat of the water as $4350 J/(kg \cdot K)$. The uncertainty of the temperature difference is:

$$\Delta T = 6.69 \pm \sqrt{0.12^2 + 0.13^2} = 6.69 \pm 0.18\,^{\circ}\mathrm{C} \tag{A.4}$$

Subsequently, the absorbed heat in the solar field and its uncertainty is:

$$\dot{Q}_{abs,meas} = \dot{m} \cdot C_p \cdot \Delta T = 1.61 \cdot 4350 \cdot 6.69 = 46917.37 W \tag{A.5}$$

$$U_{q.abs} = \pm 46917.37 \cdot \sqrt{\left(\frac{0.18}{6.69}\right)^2 + \left(\frac{0.01}{1.61}\right)^2} = \pm 1301.21 W \tag{A.6}$$

$$\dot{Q}_{abs} = 46917.37 \pm 1301.21 W \tag{A.7}$$

The energy absorbed and its related uncertainty are both integrated during a period. The procedure demonstrated above was used to calculate the uncertainty of the variables involved in the heat generated and its uncertainty.

References

[1] IEA, "International Energy Agency (IEA) - Data and Statistics." Accessed: Jan. 21, 2023. [Online]. Available: https://www.iea.org/data-and-statistics.
[2] C. Vannoni, R. Battisti, and S. Drigo, "Task 33/IV-Potential for Solar Heat in Industrial Processes Potential for Solar Heat in Industrial Processes Task 33/IV-Potential for Solar Heat in Industrial Processes," 2008.
[3] M. Abedi, X. Tan, P. Saha, J.F. Klausner, A. Bénard, Design of a solar air heater for a direct-contact packed-bed humidification–dehumidification desalination system, Appl. Therm. Eng. 244 (July 2024) (2023), https://doi.org/10.1016/j.applthermaleng.2024.122700.
[4] E. Bellos, A. Arabkoohsar, P. Lykas, C. Sammoutos, A. Kitsopoulou, C. Tzivanidis, Investigation of a solar-driven absorption heat transformer with various collector types for industrial process heating, Appl. Therm. Eng. 244 (May) (2024) 122665, https://doi.org/10.1016/J.APPLTHERMALENG.2024.122665.
[5] Y.G. Hiben, M. Bayray, J. Lauwaert, Optimizing solar-assisted industrial heating and cooling system for cost-effective installation, Appl. Therm. Eng. 230 (July) (2023) 120778, https://doi.org/10.1016/J.APPLTHERMALENG.2023.120778.
[6] A.K. Sharma, C. Sharma, S.C. Mullick, T.C. Kandpal, Solar industrial process heating: A review, Renew. Sustain. Energy Rev. 78 (January) (2017) 124–137, https://doi.org/10.1016/j.rser.2017.04.079.
[7] A.A. de la I.S. BSW-Solar, Calor Solar Para La Industria, Solar Payback (2017) 18.
[8] P. Horta and FhG ISE, "Solar IEA SHC Task 49 SolarPACES Annex IV Solar Process Heat for Production and Advanced Applications Process Heat Collectors: State of the Art and available medium temperature collectors", Accessed: Apr. 02, 2024. [Online]. Available: www.iea-shc.org.
[9] C. Valenzuela, C. Felbol, G. Quiñones, L. Valenzuela, S.L. Moya, R.A. Escobar, Modeling of a small parabolic trough plant based in direct steam generation for cogeneration in the Chilean industrial sector, Energy Convers Manag 174 (June) (2018) 88–100, https://doi.org/10.1016/j.enconman.2018.08.026.

[10] İ.H. Yılmaz, M.S. Söylemez, R. Yumrutaş, Experimental analysis and dynamic simulation of a solar-assisted industrial process using parabolic trough solar collectors under outdoor conditions, Energy Sustain. Dev. 72 (December 2023) (2022) 212–229, https://doi.org/10.1016/j.esd.2022.12.017.
[11] A.A. Hachicha, I. Rodríguez, R. Capdevila, A. Oliva, Heat transfer analysis and numerical simulation of a parabolic trough solar collector, Appl. Energy 111 (2013) 581–592, https://doi.org/10.1016/j.apenergy.2013.04.067.
[12] D. Barlev, R. Vidu, P. Stroeve, Innovation in concentrated solar power, Sol. Energy Mater. Sol. Cells 95 (10) (2011) 2703–2725, https://doi.org/10.1016/j.solmat.2011.05.020.
[13] L. Kumar, M. Hasanuzzaman, N.A. Rahim, Global advancement of solar thermal energy technologies for industrial process heat and its future prospects: A review, Energy Convers Manag 195 (February) (2019) 885–908, https://doi.org/10.1016/j.enconman.2019.05.081.
[14] W. Weiss and M. Spörk-Dür, "Solar Heat Worldwide 2022. Global Market Development and Trends 2021. Detailed Market Figures 2020," p. 87, 2022.
[15] European Commission, "CORDIS FP7 - INSUN Project - Industrial Process Heat by Solar Collectors." Accessed: Feb. 14, 2023. [Online]. Available: https://cordis.europa.eu/project/id/296009/es.
[16] A. Vittoriosi, R. Fedrizzi, R. Brock, F. Orioli, V. Orioli, D. Pietruschka, Monitoring of a MW class solar field set up in a brick manufacturing process, Energy Procedia 48 (2014) 1217–1225, https://doi.org/10.1016/j.egypro.2014.02.138.
[17] D. Pietruschka, I. Ben Hassine, M. Cotrado, R. Fedrizzi, M. Cozzini, Large scale solar process heat systems -planning, realization and system operation, Energy Procedia 91 (2016) 638–649, https://doi.org/10.1016/j.egypro.2016.06.223.
[18] European Commission, "Forthcoming Research and Industry for Eropean and National Developement of SHIP - FRIENDSHIP." Accessed: Apr. 03, 2023. [Online]. Available: https://friendship-project.eu/.
[19] European Commission, "Solar Heat for Industrial Process towards Food and Agro Industries commitment in Renewables - SHIP2FAIR." Accessed: Apr. 03, 2023. [Online]. Available: http://ship2fair-h2020.eu/.
[20] M. Mokhtar, M. Berger, C. Zahler, D. Krüger, H. Schenk, R. Stieglitz, Direct steam generation for process heat using fresnel collectors, Int. J. Thermal Environ. Eng. 10 (1) (2015) 3–9, https://doi.org/10.5383/ijtee.10.01.001.
[21] M. Berger, M. Meyer-Grünefeldt, D. Krüger, K. Hennecke, M. Mokhtar, C. Zahler, First year of operational experience with a solar process steam system for a pharmaceutical company in Jordan, Energy Procedia 91 (Jun. 2016) 591–600, https://doi.org/10.1016/j.egypro.2016.06.209.
[22] A. Frein, M. Motta, M. Berger, C. Zahler, Solar DSG plant for pharmaceutical industry in Jordan: Modelling, monitoring and optimization, Sol. Energy (2018), https://doi.org/10.1016/j.solener.2018.07.072.
[23] D. Krüger *et al.*, "Experiences with industrial solar process steam generation in Jordan," *AIP Conf Proc*, vol. 1850, no. June, 2017, doi: 10.1063/1.4984570.
[24] Solatom CSP, "SolatomCSP." Accessed: Jun. 08, 2020. [Online]. Available: http://www.solatom.com/.
[25] INDERTEC, "Indertec desarrolla SOLPINVAP: Energía SOLar de Media Temperatura para procesos INdustriales con demanda de VAPor." Accessed: Jun. 08, 2020. [Online]. Available: https://indertec.com/2020/01/19/indertec-desarrolla-solpinvap-energia-solar-de-media-temperatura-para-procesos-industriales-con-demanda-de-vapor/.
[26] A. Zirkel-Hofer, et al., Improved in situ performance testing of line-concentrating solar collectors: Comprehensive uncertainty analysis for the selection of measurement instrumentation, Appl. Energy 184 (2016) 298–312, https://doi.org/10.1016/j.apenergy.2016.09.089.
[27] H. Coleman W. and W. Glenn Steele, *Experimentation, Validation, and Uncertainty Analysis for Engineers.*, vol. 78, no. 220. 1982.